WILEY | Hindawi

Research Article

A Miniaturized, Dual-Port, Multiband MIMO with CSRR DGS for Internet of Things Using WLAN Communication Standards

Rashmi Roges [1,2] **Praveen Kumar Malik,** [1] **Sandeep Sharma,** [2] **Sandeep Kumar Arora,** [1] **and Fidele Maniraguha** [3]

[1]*Lovely Professional University, Phagwāra, India*
[2]*Bhagwan Parshuram Institute of Technology, Delhi, India*
[3]*University of Rwanda, African Center of Excellence in Internet of Things, Kigali, Rwanda*

Correspondence should be addressed to Praveen Kumar Malik; pkmalikmeerut@gmail.com,
Sandeep Kumar Arora; sandeep.16930@lpu.co.in, and Fidele Maniraguha; manifils@gmail.com

A compact, dual-port, triband MIMO antenna is designed and tested for three sub-6 GHz WLAN bands for IoT applications. The size and performance of the antenna make it versatile for the emerging IoT applications communicating using the 2.4 GHz, 5.2 GHz, and 5.8 GHz WLAN frequencies. The single radiating element of antenna geometry includes a pair of modified and optimized rectangular patches. A complimentary split ring resonator (CSRR) structure is incorporated in the ground plane as a defect (defected ground structure) to attain the third operational band. The orientation of the elements, orthogonally arranged, along with DGS, enhances the isolation between the radiating elements keeping it below 18 dB throughout the three operating frequency bands. The size of the final antenna is as small as $0.32\lambda_0 \times 0.32\lambda_0$ mm^2 build on commercially available and cheap FR4 substrate of thickness 1.5748 mm. A peak gain of 7.17 dBi is attained for the proposed MIMO system. This MIMO antenna also satisfies the diversity parameter requirements including DG > 9.8, ECC < 0.5, TARC < −10 dB, and CCL < 0.5 bits/s/Hz. This makes the proposed antenna a good candidate for IoT applications employing WLAN frequencies.

1. Introduction

The present decade has seen an overwhelming interest in IoT technology, which is an extension of worldwide web. The web now includes all devices connected to the internet through the "Internet of Things" technology. The efficient and reliable communication between all the devices connected to the internet has ensured a massive number of applications where its benefits can be exploited. The applications include road traffic control and vehicular IoT [1–3], industrial IoT [4–6], and medical IoT [7, 8]. This further pushed the antenna researchers to provide wireless solutions which can provide a functional platform for more than one application [9]. Some major requirements of IoT applications are to maintain a good quality of signal, device compatibility, multifunctionality, and reliability.

WLAN is the wireless solution which enables flexibility and user mobility [10]. WLAN is also one among the most common communication technology which is profoundly applied in IoT applications. The operational bands for WLAN include 2.4 GHz, (2.4-2.484 GHz), 5.2 GHz, (5.15-5.25 GHz), and 5.8 GHz, (5.725-5.825 GHz). The lower band covers the low-bandwidth applications within medium range and the upper bands supports low-range, higher-bandwidth applications [11]. Compared to the traditional communication solutions, MIMO systems are the future of present-day communication technology despite its additional cost and complexity. The three significant features of MIMO, which makes it unique and popular are its beam steering capability, the enhanced data capacity, and the diversity characteristics [12, 13]. The major challenge faced in the modern-day MIMO design are in integrating multiple radiating elements in limited space with good isolation and attaining a low correlation
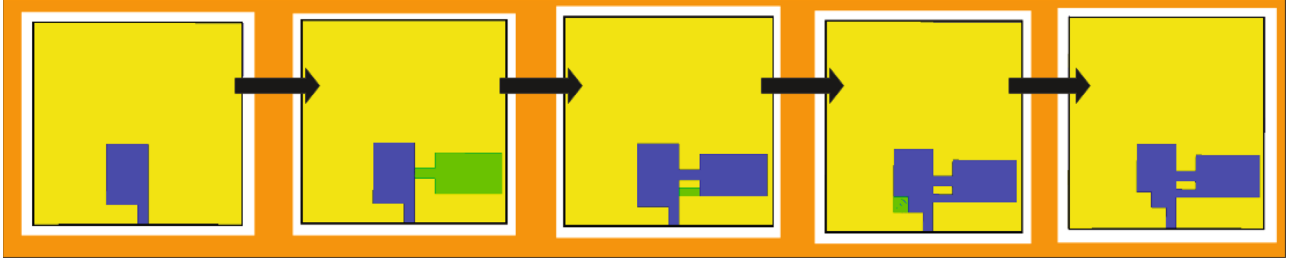
FIGURE 1: Evolution stages of the radiating element.

between the closely placed antenna elements. Inclusion of lower WLAN band greater influences the size of the antenna, and additionally, a MIMO system needs to have enough spacing between the radiation elements to avoid mutual coupling between the elements [14–17].

Inclusion of the lower WLAN frequency while maintaining the compactness and isolation in a MIMO antenna system is a hard task for an antenna design engineer. The antennas in the literature includes the lower band at the cost of size [18–22] or low isolation [23]. [24] refers to a miniaturized antenna of size 12.5 mm × 12.5 mm for upper range of frequency (mm range of 35 GHz), and [25] proposes the use of decoupling structure (isolation > 14 dB) in the design of a closely placed MIMO antenna elements for 5.4 GHz of size 44 mm × 37 mm. The novelty of the proposed structure is the achievement of a compact size and high isolation (>18 dB for lower band and >23 dB for upper bands), irrespective of inclusion of the lower band of operation (2.4 GHz). This paper proposes a compact 2-port, triband MIMO antenna for WLAN IoT applications with high isolation, simple and compact structure, good gain, and radiation characteristics. The fine tuning of the antenna to 2.4 GHz, 5.2 GHz, and 5.8 GHz is an additional advantage of this design.

2. Antenna Design and Dimensions

The evolution stages of the design in shown in Figure 1, and the single radiating element of the 2-port MIMO system is as shown in Figure 2. Low-cost easily available FR4 substrate is used for the fabrication, and high-frequency structure simulator (HFSS) software is used for the design and analysis of the antenna. The overall dimension of the final antenna is 40 mm × 40 mm × 1.5748 mm.

It consists of five stages as shown in Figure 1. The study starts with stage-1, in which, a rectangular microstrip antenna of size $L_9 \times W_7$ is designed at WLAN frequency.

The dimensions of rectangular patch antenna are calculated from the following equations:

$$W_7 = \frac{c}{2f_d} \sqrt{\frac{2}{\varepsilon_r + 1}}, \qquad (1)$$

where W_7 is the width of the patch, c is the speed of light in free space, f_d is the design frequency, and ε_r is the substrate's dielectric constant.
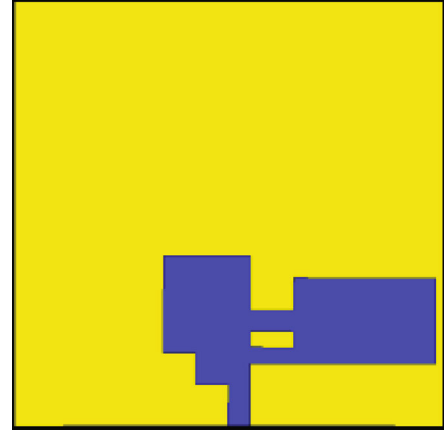

FIGURE 2: The antenna geometry of the radiating single element.

The length L_9 of the rectangular base structure is calculated as

$$L_9 = \frac{\lambda_0}{2f_d \sqrt{\varepsilon_{\text{eff}}}} - 2\Delta L, \qquad (2)$$

where L_9 is the length of the patch, λ_0 is the wavelength in free space, and ΔL is the fringing length. The effective dielectric constant ε_{eff} of structure is calculated by (3), and Fringing length ΔL is calculated as in (4).

$$\varepsilon_{eff} = \frac{\varepsilon_r + 1}{2} + \frac{\varepsilon_r - 1}{2} \left(1 + 12 \frac{h}{w} \right)^{-0.5}, \qquad (3)$$

$$\Delta L = 0.412h \frac{(\varepsilon_{\text{eff}} + 0.3)((w/h) + 0.264)}{(\varepsilon_{\text{eff}} + 0.254)((w/h) + 0.8)}. \qquad (4)$$

The width of the feedline is calculated from Equation (5) for 50 Ω characteristics impedance (Z_0) as

$$\frac{W_4}{h} = \frac{2}{\pi} \left\{ B - 1 - \ln(2B - 1) + \frac{\varepsilon_r - 1}{2\varepsilon_r} \left[\ln(B - 1) + 0.39 - \frac{0.61}{\varepsilon_r} \right] \right\}, \qquad (5)$$

where

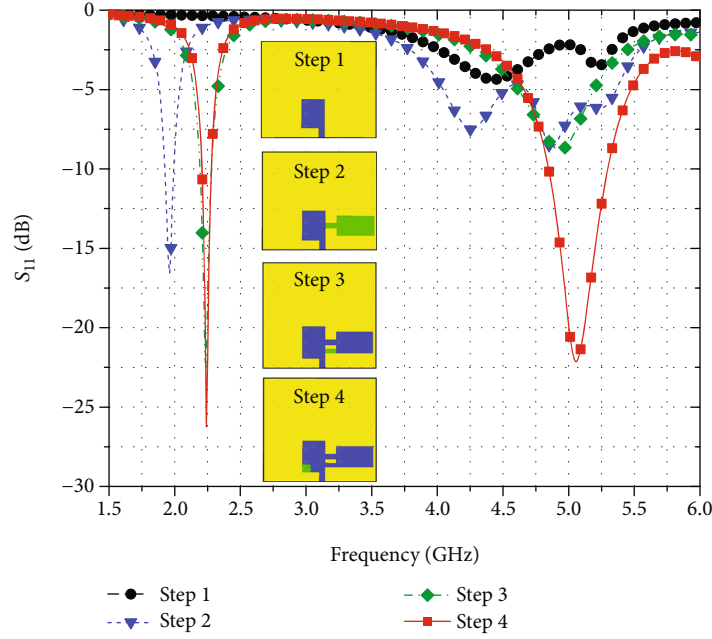$$B = \frac{377\pi}{2Z_0 \sqrt{\varepsilon_r}}. \qquad (6)$$

FIGURE 3: Evolution of the basic radiating element and the corresponding S parameter plot.

The basic patch gave no significant bandwidth over the minimum threshold of -10 dB return loss. The second step added another rectangular patch to the right side of the first patch. This helped in achieving a single narrow band (1.922 GHz–2.009 GHz) resonating at 1.953 GHz with a return loss of 23.71 dB. An additional band is observed around 5 GHz but it is not below -10 dB. In the following step, an addition connect was offered to the first and second rectangular patches. This helped in shifting the bandwidth to the right to (2.18 GHz-2.286 GHz) resonating at 2.235 GHz with -36.244 dB. A shift is observed in the additional bandwidth seen in step two but the return loss could not be enhanced in this step. In step 4, a square slot of 3 mm × 3 mm was cut in the right corner of the first rectangular patch. This provided an enhanced return loss to the additional operation band. The final resonating element has dual operational bandwidths, 2.207 GHz-2.28 GHz and 4.849 GHz-5.249 GHz resonating at 2.235 GHz and 5.04 GHz, respectively. The summary of S_{11} for the evolutionary stages is given in Figure 3.

The parametric study is conducted on every element added in each step of progress to the final radiating element. In step 2, the length and position of the second rectangular patch added is optimized through parametric study as shown on Figure 4(a). The results of the study on step two is given in Figures 4(b) and 4(c).

In step 3 of the design of radiating element, a rectangular stub is used to make an extra connection with the first and second rectangular patch. The width of this patch is set under parametric study to conclude that the best return loss characteristics is attained at 2.4 GHz when the width of the stub is 1.5 mm. The diagrammatic representation of the parametric analysis done on step 3 is shown in Figure 5.

In the final step of the design, a slot is embedded in the first rectangular patch. Embedding this slot results in two

operating bands. The first band ranged between 2.207 GHz and 2.28 GHz, and the second band from 4.84 GHz to 5.24 GHz. The length and width of the slot embedded are again optimized through parametric study. Figure 6(a) shows the parameters investigated under this study, Figure 6(b) shows the parametric analysis on length of the slot, and Figure 6(c) shows the parametric study on the width of the slot.

The radiating element was thus designed. Further, a 2-element MIMO system was designed as shown in Figure 7. Individual radiating elements were organized in an FR4 substrate of size 40 mm × 40 mm. The MIMO antenna with tri-band evolved through three stages, stage 1 is named Ant_I and is shown in Figure 7(a). In the next stage, two-element MIMO is configured by placing the elements orthogonally to use antenna utilization to enhance isolation. This antenna is names as Ant_II and is shown in Figure 7(b). In stage 3, a CSRR is embedded into the ground plane to achieve the third band of resonance and improve isolation. Stage 3, with CSRR in DGS, is named as Ant_III as shown in Figure 7(c). The final top and bottom view of the antenna is shown in Figures 7(d) and 7(e), respectively. The optimized design dimensions are summarized in Figure 8(a) and Table 1.

CSRR is used as an effective method to achieve compactness while designing for a particular frequency. CSRR can be excited by means of an axial time varying electric field or by means of a magnetic field applied to the plane of antenna. Under ideal conditions, i.e., a perfectly conducting and zero-thickness metallic surface, it can be demonstrated that the resonance frequency of the CSRR is identical to the resonance frequency of the SRR (provided identical dimensions and substrate are considered). Indeed, the capacitance of the CSRR, C_c, is the capacitance of a disk of radius $r_o - c/2$ surrounded by a ground plane at a distance c of its edge. The inductance is

(a)

Positon of the second rectangle

- L_4 = 6 mm L_4 = 10 mm
- L_4 = 7 mm L_4 = 11 mm
- L_4 = 8 mm L_4 = 12 mm
- L_4 = 9 mm

(b)

Length of the second rectangle

- W_1 = 8 mm W_1 = 11 mm
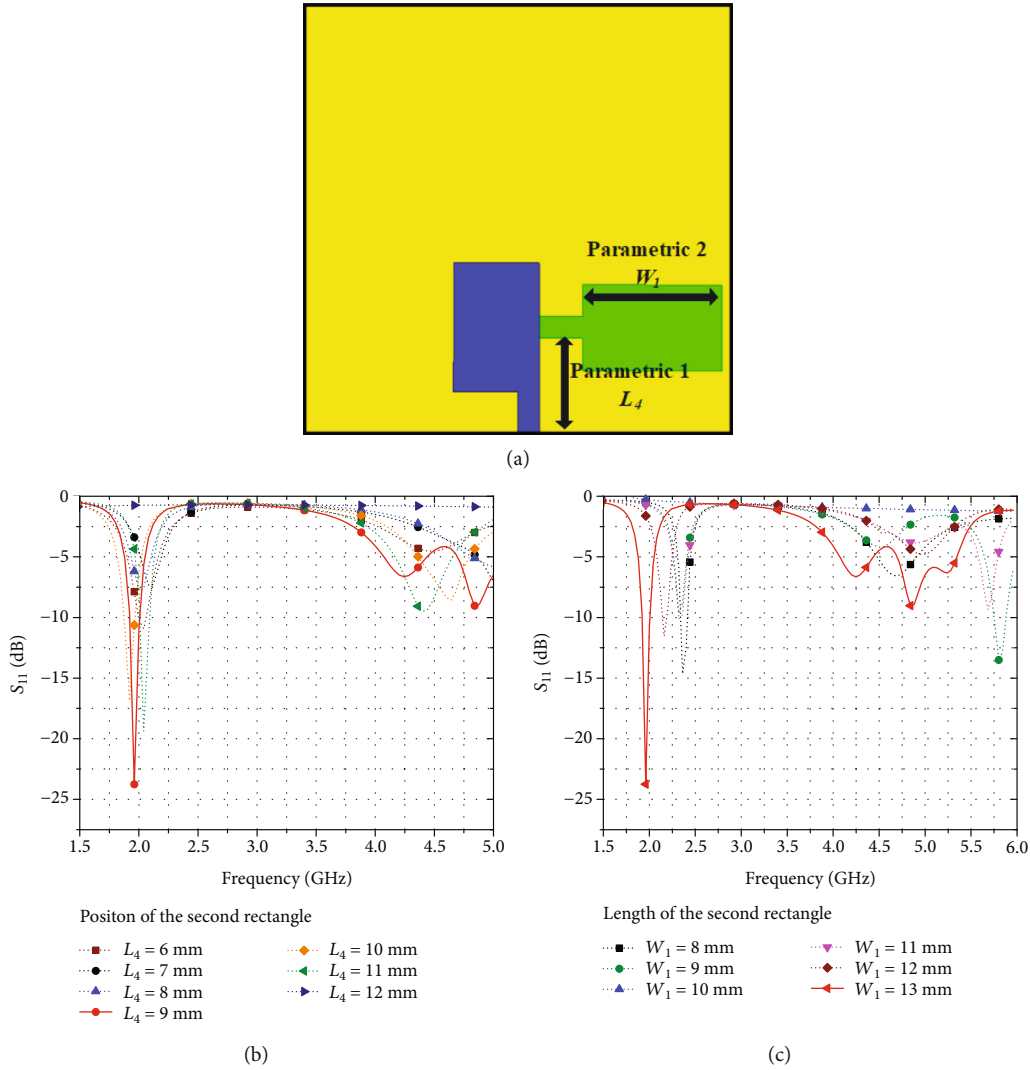- W_1 = 9 mm W_1 = 12 mm
- W_1 = 10 mm W_1 = 13 mm

(c)

FIGURE 4: Parametric study done on step 2. (a) Antenna dimensions where parametric study is applied. (b) Parametric analysis results on position of the second rectangle. (c) Parametric study results on length of the second rectangle.

- L_3 = 0.1 mm L_3 = 1 mm
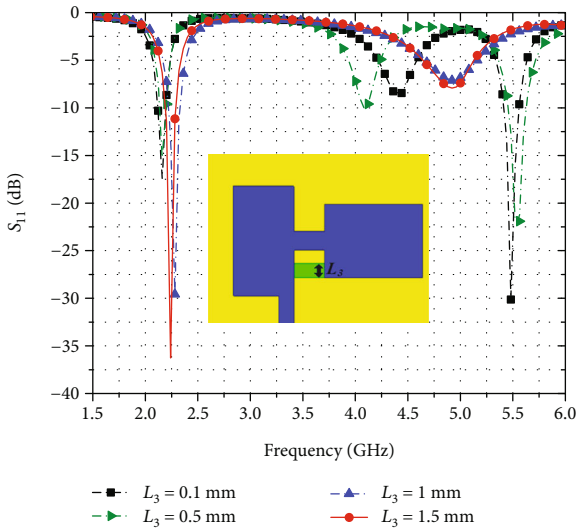- L_3 = 0.5 mm L_3 = 1.5 mm

FIGURE 5: Parametric study done on the width of the rectangular stub connecting the two rectangular patches.

given by the parallel connection of the two inductances of the metallic strips connecting the inner and outer metallic regions of the CSRR. These inductive values are given by $L_o/2$, where $L_o = 2\pi r L_{pul}$, with L_{pul} being the per unit length inductance. Due to change in equivalent inductance and capacitance of the ground plane, effective current distribution of ground plane changes resulting in the appearance of a new ISM band (5.119 GHz–5.353 GHz). The CSRR parameters include the average ring of radius r_o, i.e., the mean radius of the ring, and ring width c as shown in Figure 8(b).

CSRR characteristics have been widely exploited by antenna designers to achieve various desired parameters. It has seen to be used in literature to achieve lower resonant frequencies in miniaturized antenna [26], to realize bandpass and bandstop filters [22, 27], to enhance isolation in MIMO antenna systems, [28], and so on. The circuit models corresponding to CSRR are not very accurate because circuit modal of unit cell must take into account the coupling between the resonator and the line, i.e., interresonator
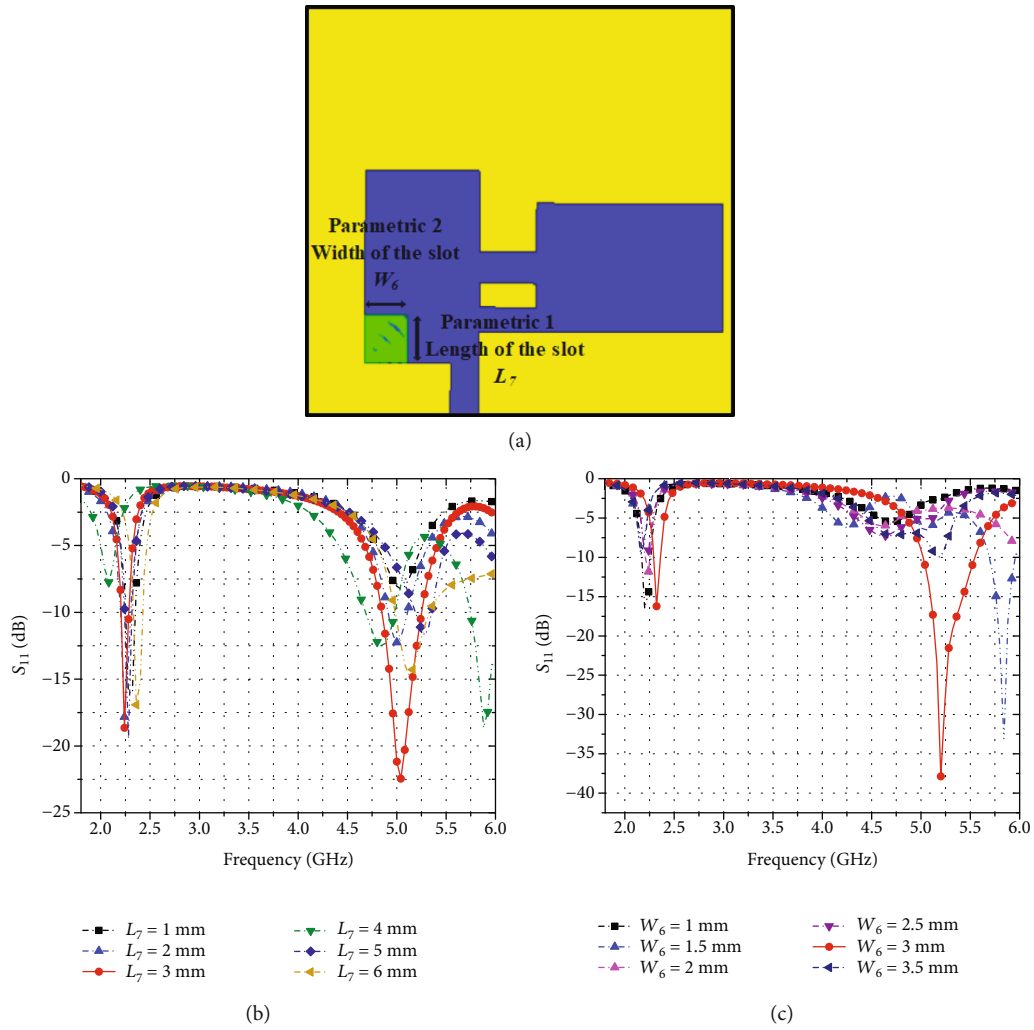
(a)

(b)

(c)

FIGURE 6: Parametric analysis done on the slot on the rectangular radiating patch. (a) Figure showing the parameters under study for optimization. (b) Parametric analysis results on length of the slot. (c) Parametric study results on width of the slot.
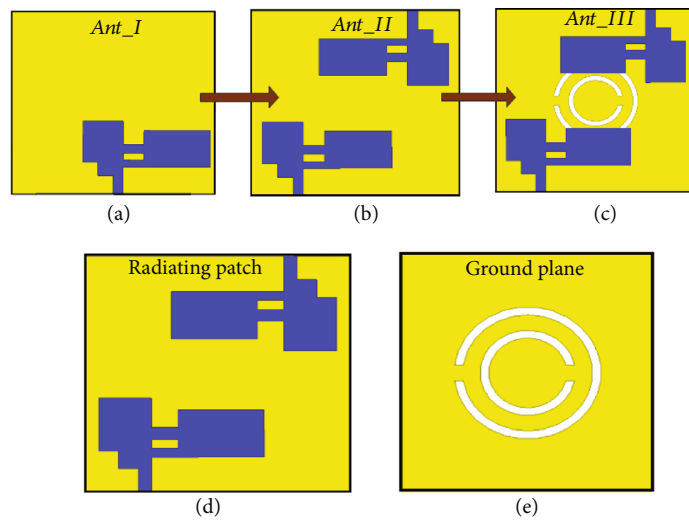

(a)　(b)　(c)

(d)　(e)

FIGURE 7: Evolution of the dual-port triband MIMO antenna. (a) Radiating single element as Ant_I. (b) Orthogonally placed 2-element MIMO, Ant_II. (c) Two-element MIMO with CSRR in DGS, Ant_III. (d) Radiating plane of the proposed antenna. (e) Ground plane of the proposed antenna.
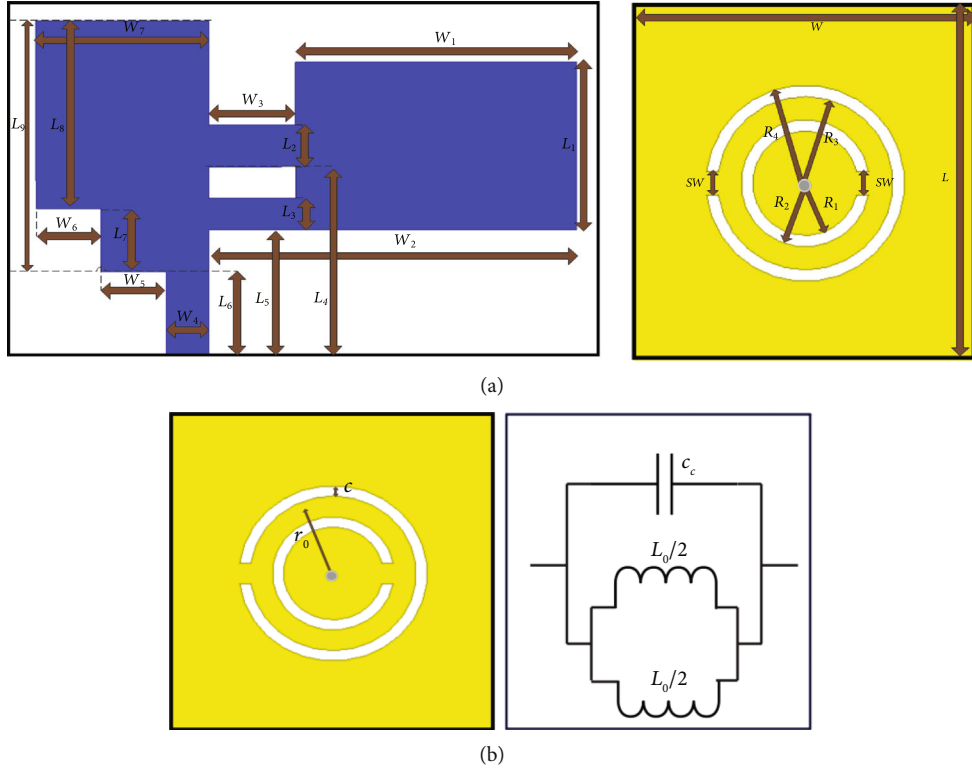
(a)

(b)

FIGURE 8: (a) Design dimensions for the patch and ground plane. (b) CSRR dimensions and its equivalent circuit.

TABLE 1: Optimized dimensions of the patch and ground plane of the proposed MIMO antenna.

(a)

W	W_1	W_2	W_3	W_4	W_5	W_6	W_7
40 mm	13 mm	17 mm	4 mm	2 mm	3 mm	3 mm	8 mm

(b)

L	L_1	L_2	L_3	L_4	L_5	L_6	L_7	L_8	L_9
40 mm	8 mm	2.54 mm	1.55 mm	9 mm	6 mm	4 mm	3 mm	9 mm	12 mm

(c)

R_1	R_2	R_3	R_4	SW	r_o	c
4.5 mm	5.5 mm	7.5 mm	8.5 mm	2 mm	5 mm	1 mm

coupling. In addition to this, the decrease in electrical size of the CSRR is seen to have an effect in narrowing the operational bandwidth.

Figures 9 and 10 picturize the operational bandwidths and isolation achieved in each stage of evolution. *Ant_I* shows two operational bandwidths, 2.207 GHz to 2.28 GHz, resonating at 2.235 GHz (-18.48 dB) and 4.84 GHz to 5.04 GHz, resonating at 5.04 GHz (-22.31 dB). *Ant_II* is the orthogonally placed 2-element MIMO system with two bands of 2.299 GHz to 2.360 GHz and 5.806 GHz to 6.334 GHz. The return loss of the second band originally present in the simulation results of *Ant_I* was reduced below the reference level of -10 dB. So, the

two bands of Ant_II resonated at 2.32 GHz (-11.45 dB) and 6.121 GHz (-18.879 dB), respectively. The addition of CSRR as a DGS to *Ant_II* attained enough return loss (>-10 dB) for the second band of *Ant_I*. *Ant_III*, therefore, has three bands of operation as 2.336 GHz to 2.449 GHz, resonating at 2.4 GHz (-20.17 dB); 5.696 GHz to 6.29 GHz, resonating at 5.8 GHz (-40.03) similar to that of *Ant_II*; and the third additional band (as in *Ant_I*) 5.119 GHz to 5.353 GHz, resonating at 5.2 GHz (-33.16 dB).

Figure 10 shows the isolation between the elements in *Ant_II* (without CSRR) and *Ant_III* (with CSRR). For band 1 (2.336 GHz–2.449 GHz), the isolation ranges between
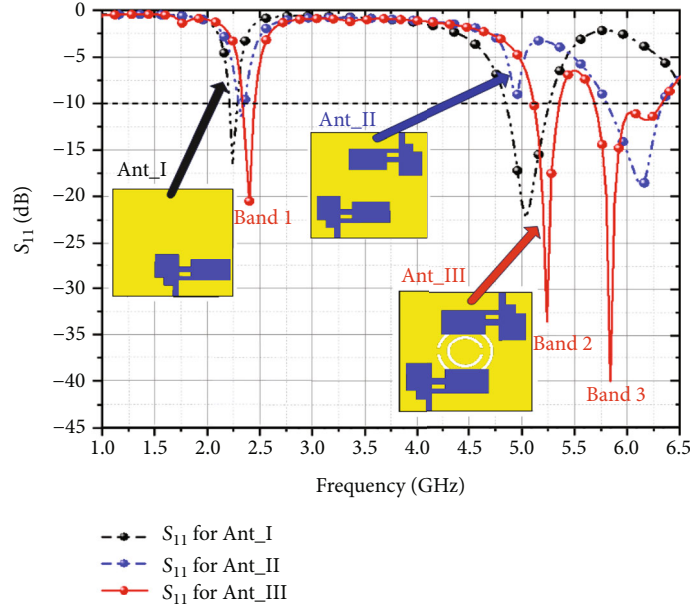
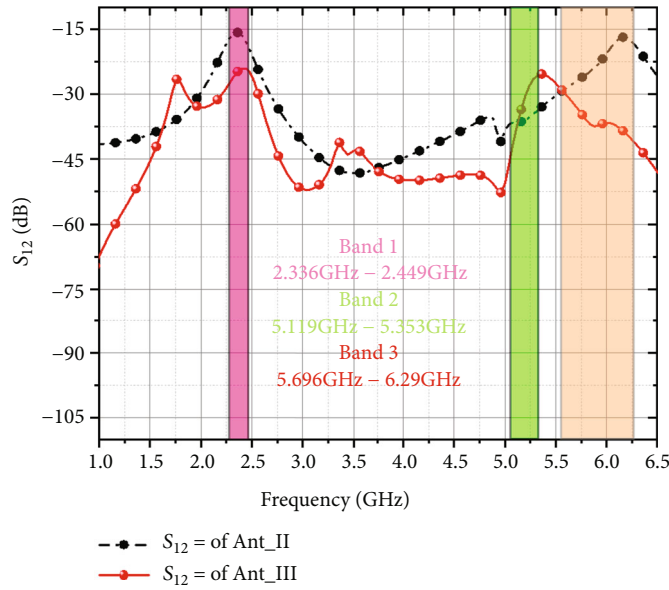FIGURE 9: S_{11} evolutional stages of the compact two-element triband MIMO.

FIGURE 10: Isolation of *Ant_II* and *Ant_III*.

-15.97 dB and -18.87 dB in *Ant_II* and -24.05 dB and -25.94 dB in *Ant_III*. At the first resonance (2.39 GHz), the isolation in *Ant_II* is -16.32 dB and in *Ant_III* is -24.05 dB. For the second band (5.119 GHz–5.353 GHz), the isolation ranges between -32.94 dB and -36.54 dB in *Ant_II* and -41.36 dB and -25.38 dB in *Ant_III*. At the second resonance (5.235 GHz), the isolation in *Ant_II* is -35.32 dB and in *Ant_III* is -28.06 dB. For band 3 (5.696 GHz–6.29 GHz), the isolation ranges between -16.84 dB and -27.34 dB in *Ant_II* and -32.32 dB and -41.28 dB in *Ant_III*. At the third resonance (5.84 GHz), the isolation in *Ant_II* is -24.7 dB and in *Ant_III* is -37 dB. Figure 11 shows the image of the fabricated antenna.

3. Results and Discussions

A dual-element, triband MIMO antenna is designed and fabricated for measurements. The antenna offers three versatile frequencies of operation in the sub-6 GHz band for various WLAN and IoT applications. The return loss for the antenna was measured by a vector network analyzer (VNA), and the results seems to satisfactorily match with the simulated results. The performance of the MIMO antenna was also studied under an anechoic chamber to determine the gain and the radiation characteristics. Slight deviations are observed between the simulated and measured values which might be a possibility due to minute

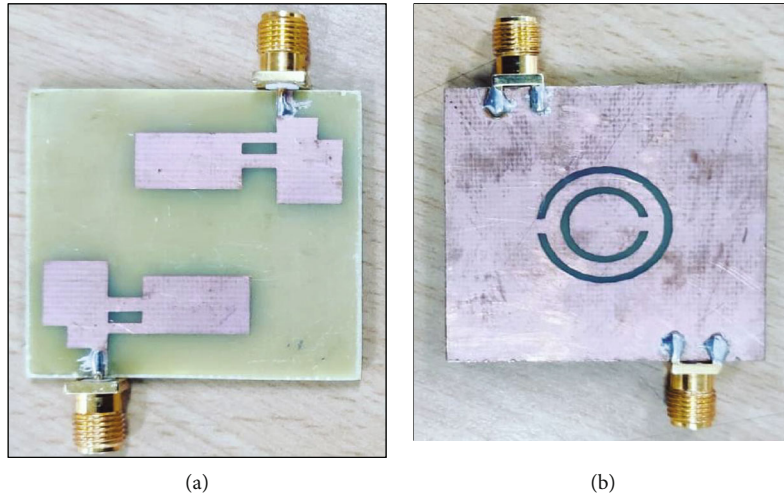(a)   (b)

FIGURE 11: The picture of the fabricated antenna. (a) Radiating patch and (b) ground plane of the proposed triband MIMO.
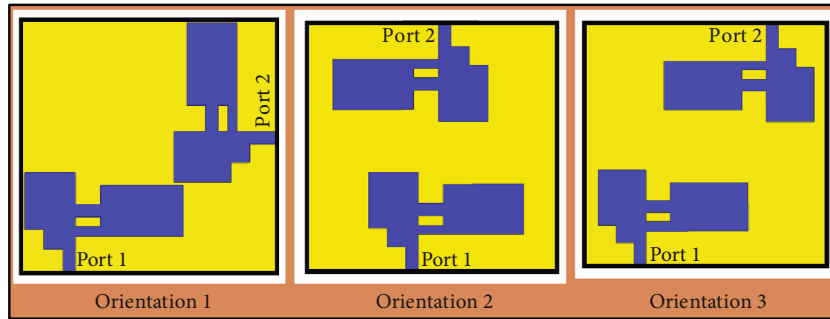

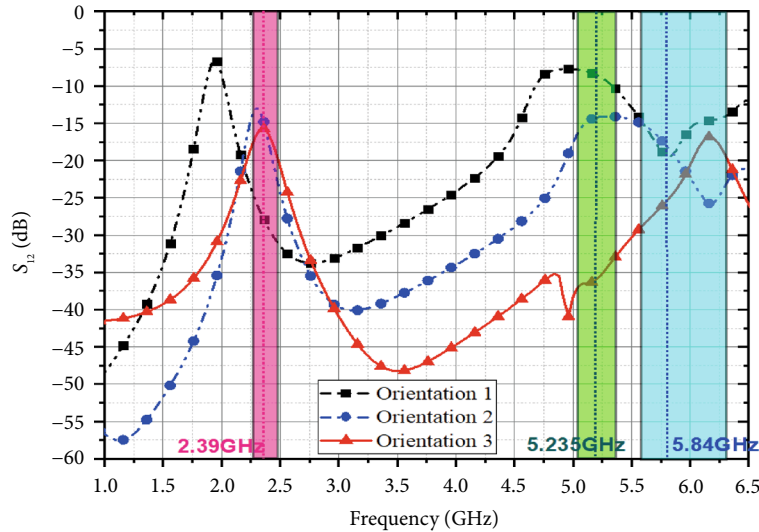FIGURE 12: Variations in orientations applied.

FIGURE 13: Isolation (dB) achieved for different orientations.

error that occurred during the fabrication, soldering process, or testing set up.

3.1. Parametric Study. A set of parametric study was conducted to attain best possible isolation between the radiating elements and to achieve all three bands of operation.
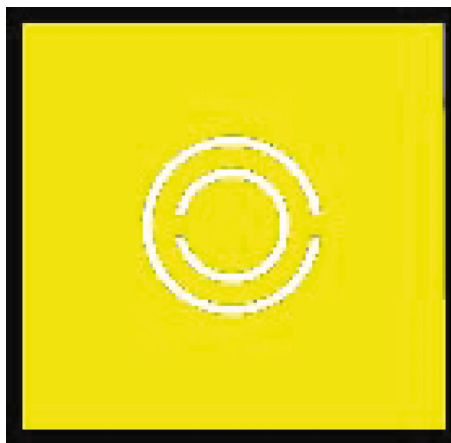
3.1.1. Orientation of the Antenna Elements. The element orientation in the substrate was carefully optimized to achieve maximum isolation. Figure 12 shows the different orientations investigated. The antenna elements were placed at 90° with respect to one another (orientation 1), at 180° with each other (orientation 2), and at 180° and moved to
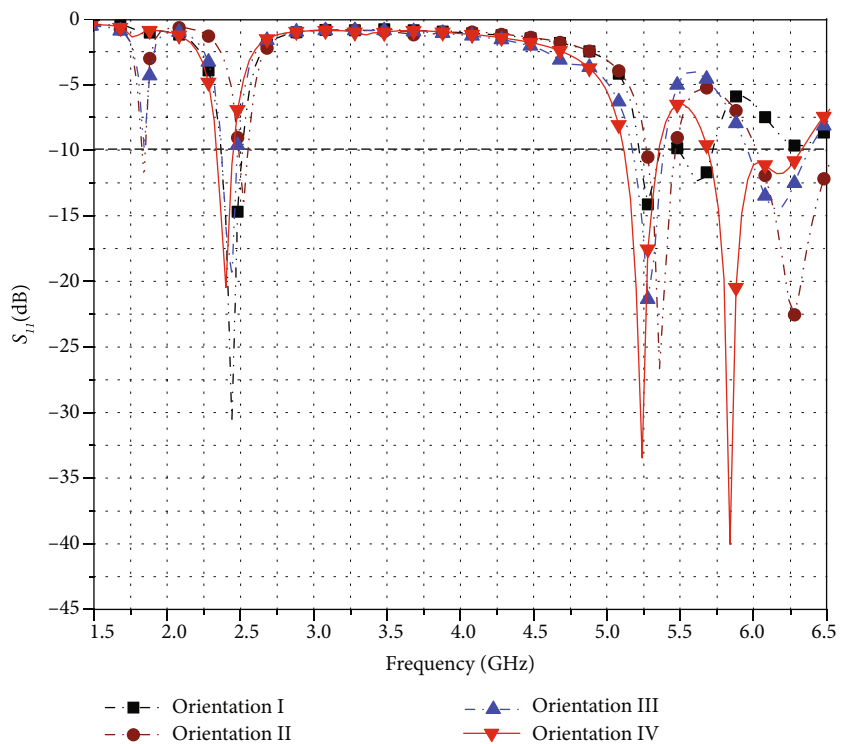
(a)
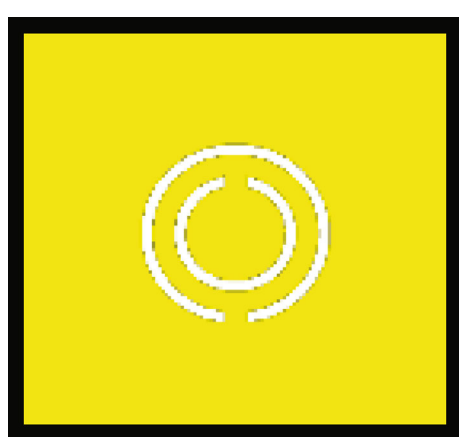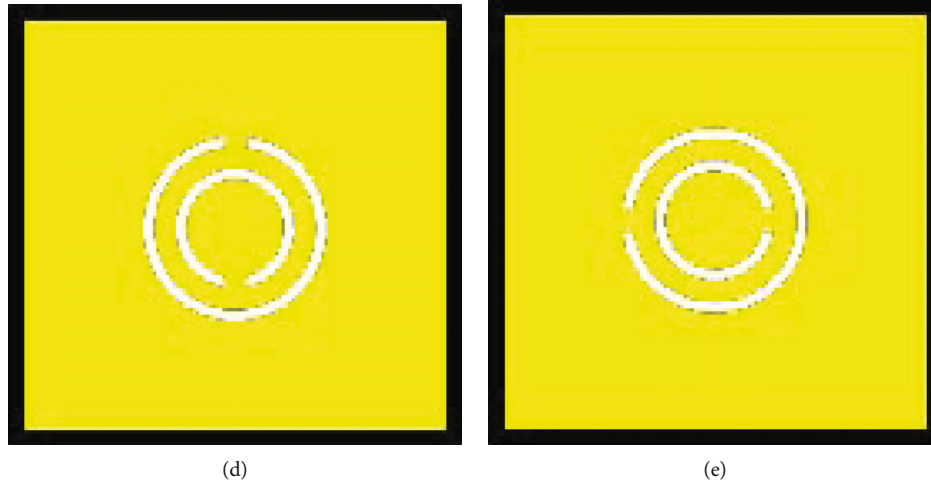

(b)

(c)

FIGURE 14: Continued.

(d)

(e)

Figure 14: The variation in S_{11} for different orientations of CSRR in the ground plane. (a) Comparison of S_{11} for 4 different orientations of CSRR. (b) Orientation I. (c) Orientation II. (d) Orientation III. (e) Orientation IV.
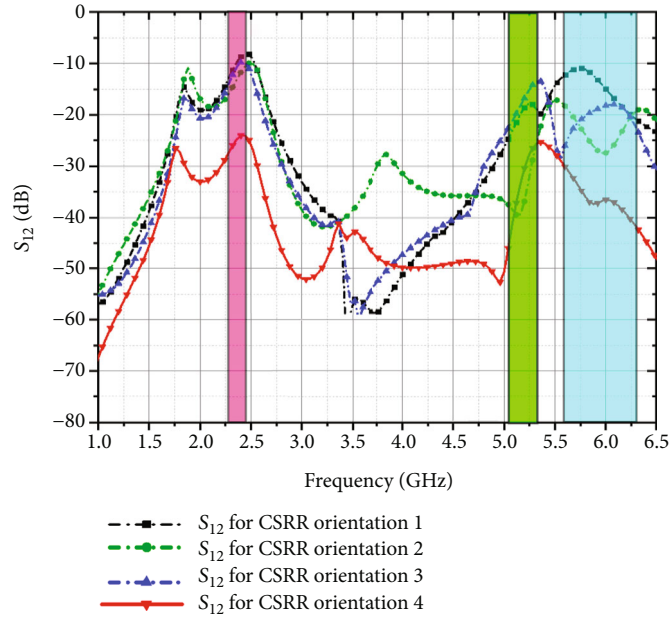

Figure 15: Isolation for different orientations of CSRR in the ground plane.

the corners to keep them maximum apart from each other (orientation 3). The orientation 1 gave good isolation at the lower band (2.33 GHz-2.44 GHz) but isolation was above -10 dB for the second band (5.11 GHz-5.35 GHz) and between -15 dB and -20 dB for the third band (5.69 GHz-6.29 GHz). Orientation 2, meanwhile, provided good isolation to (5.69 GHz-6.29 GHz) band. Orientation 3 attained lowest isolation for all the three resonant frequencies as shown in Figure 13.

The orientation of the CSRR in the ground plane of the MIMO antenna also influences the performance of the MIMO system as shown in Figure 14. Orientation I provides three operating bands but the return loss is very less for band (5.11 GHz-5.35 GHz and 5.69 GHz-6.29 GHz). Orientation

II gives a slightly shifted version of the bandwidths towards the right with an additional resonance at 1.8 GHz. The resonant frequencies in orientation II are 1.88 GHz, 2.55 GHz, 5.39 GHz, and 6.31 GHz. The third orientation attains a band at 1.8 GHz but not enough to have a return loss beyond -10 dB. The first lower band resonates at 2.43 GHz, the second at 5.28 GHz, and the third band at 6.1 GHz. The orientation of CSRR as in orientation IV optimizes the resonant frequencies to 2.38 GHz, 5.23 GHz, and 5.84 GHz. Figure 15 shows the variations in S_{12} according to the orientation of CSRR in the ground plane. At some points, it is seen that the isolation for orientation 4 is less compared to other orientation by orientation 4 shows better isolation than all other orientations for the operating bandwidths.

(a)
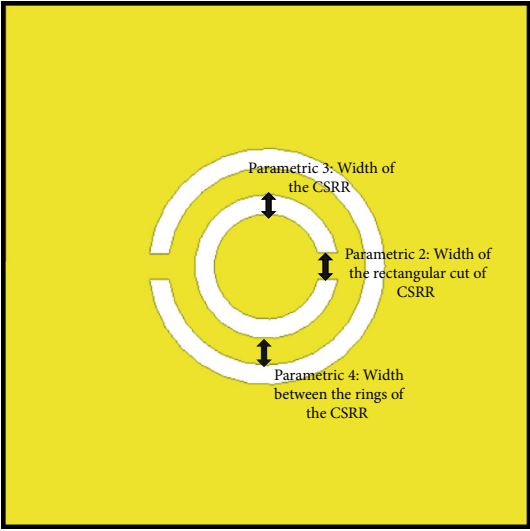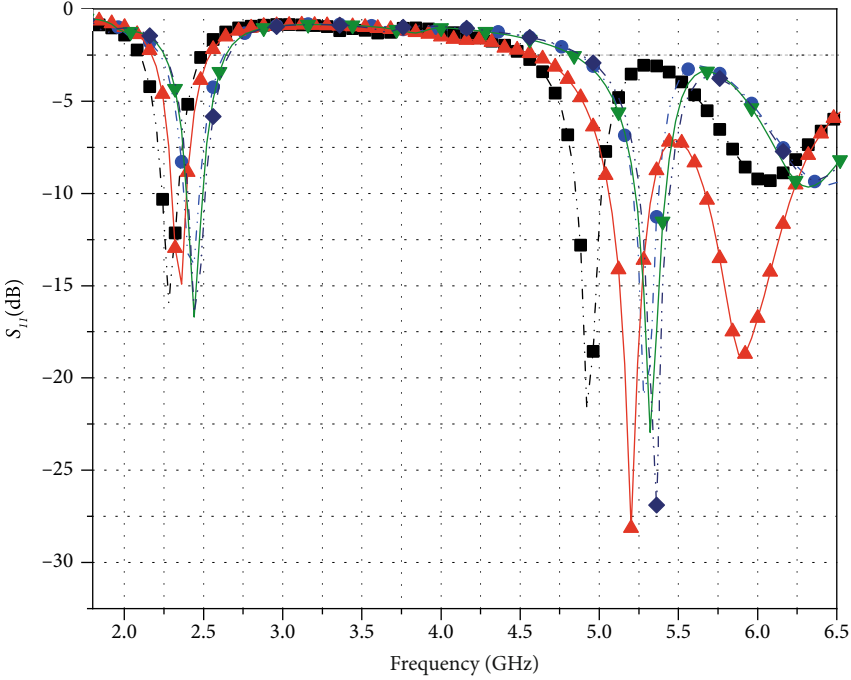
Parametric 2

(b)

FIGURE 16: Continued.
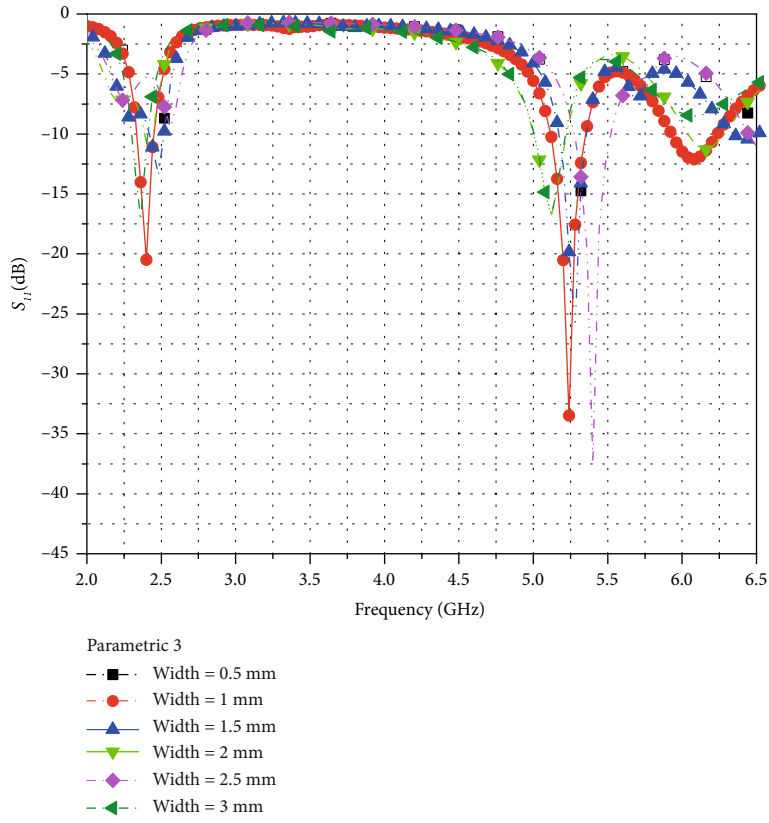
(c)
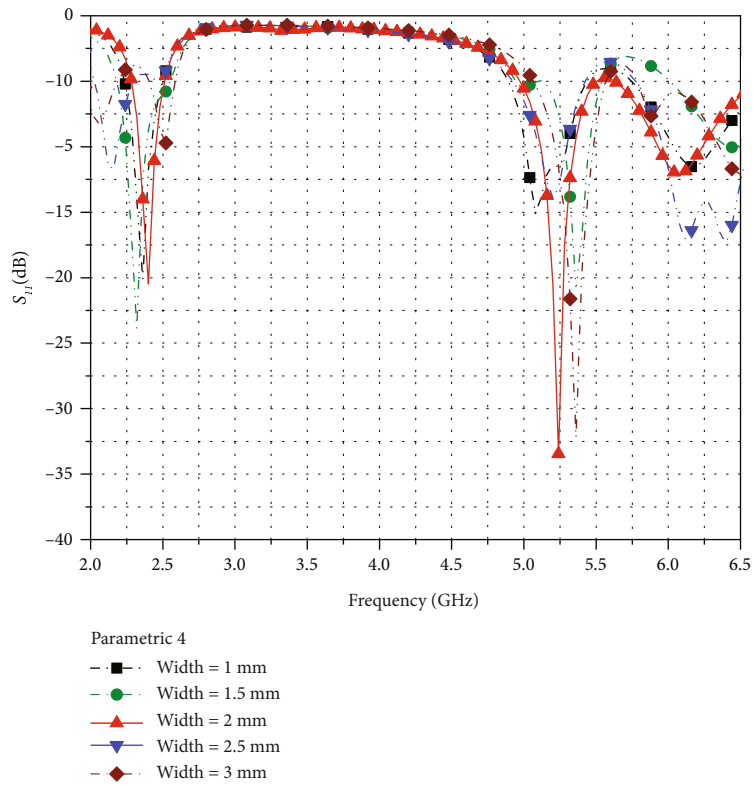
(d)

Figure 16: Parametric study on CSRR. (a) Parameters under investigation. (b) Slot width of CSRR. (c) Width of CSRR rings. (d) Spacing between the CSRR rings.

(a)

(b)

FIGURE 17: (a) Simulated and measured *S* parameters for the proposed antenna. (b) Gain and radiation efficiency for the proposed MIMO antenna.

Normalized radiation pattern at 2.4 GHz

——— Simulated E-Plane
——— Simulated H-Plane
—■— Measured E-Plane
—■— Measured H-Plane

(a)

Normalized radiation pattern at 5.2 GHz

——— Simulated E-Plane
——— Simulated H-Plane
—■— Measured E-Plane
—■— Measured H-Plane

(b)

Normalized radiation pattern at 5.8 GHz

——— Simulated E-Plane
——— Simulated H-Plane
—■— Measured E-Plane
—■— Measured H-Plane

(c)
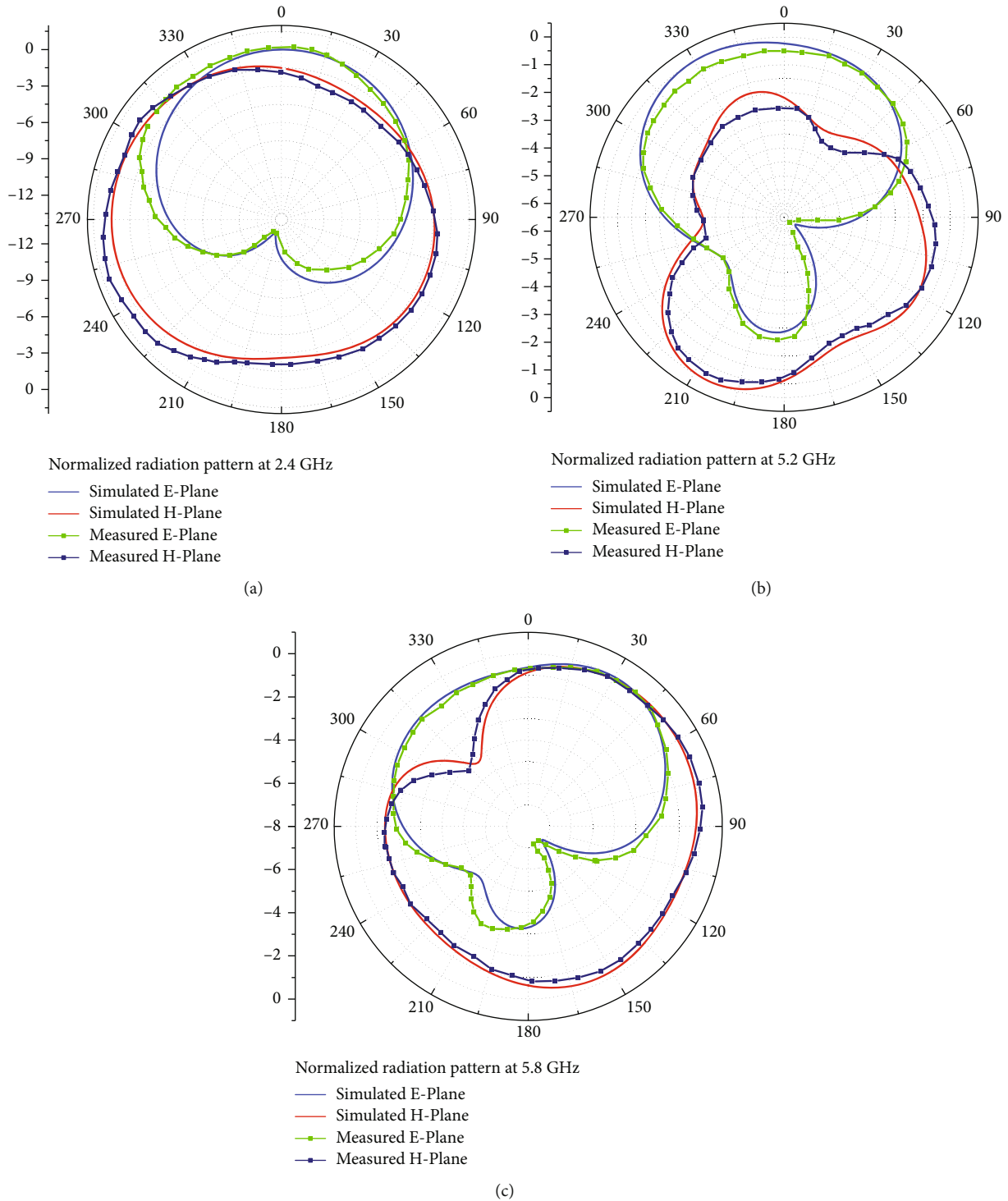
FIGURE 18: E-plane and H-plane radiation patterns. (a) At 2.4 GHz, (b) at 5.2 GHz, and (c) at 5.8 GHz.

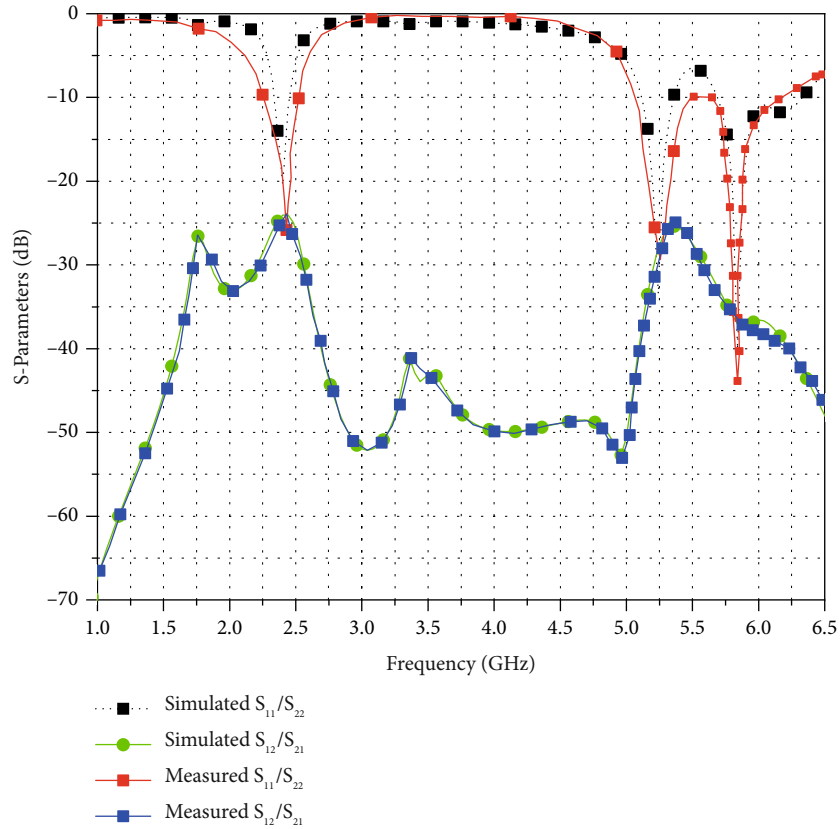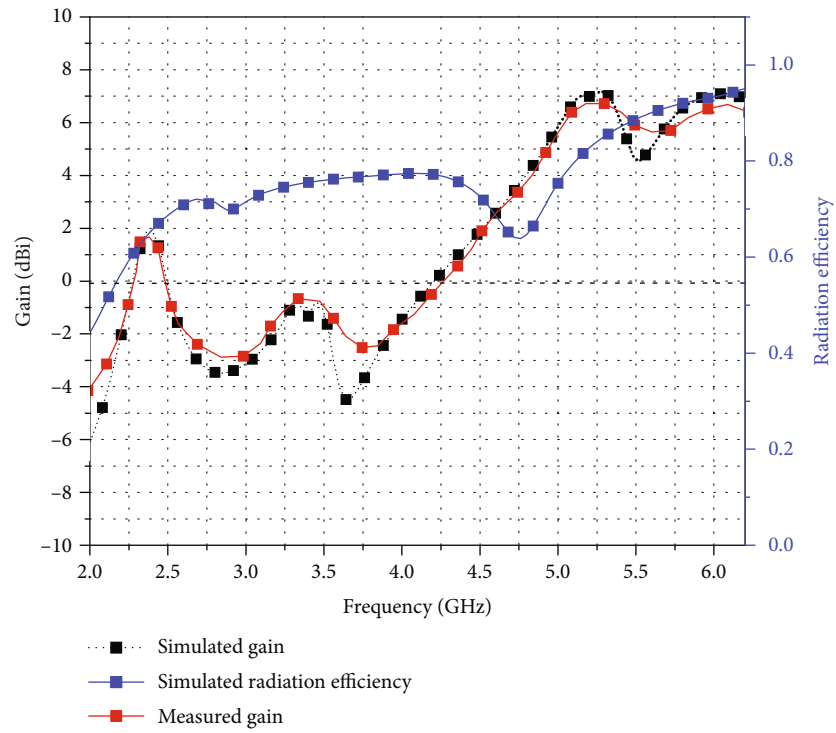The other parameters of CSRR investigated parametrically are shown in Figure 16(a). The includes the width of the rectangular slot cut on the CSRR (Figure 16(b)), the width of the rings of the CSRR (Figure 16(c)), and the distance or spacing between the rings of the CSRR (Figure 16(d)). After the parametric analysis, the slot width of CSRR is fixed at 2 mm, and the width of CSRR and spacing between the rings of CSRR are fixed at 1 mm.

3.2. Antenna Parameters. The simulated and measured values of the antenna parameters for the proposed antenna is discussed below.

3.2.1. S Parameters. The simulated and measured S parameters are in good agreement with each other. Figure 17(a) shows the summary of both return loss and isolation values for the proposed antenna.

ECC from S-Parameters

(a)

ECC from far field radiation
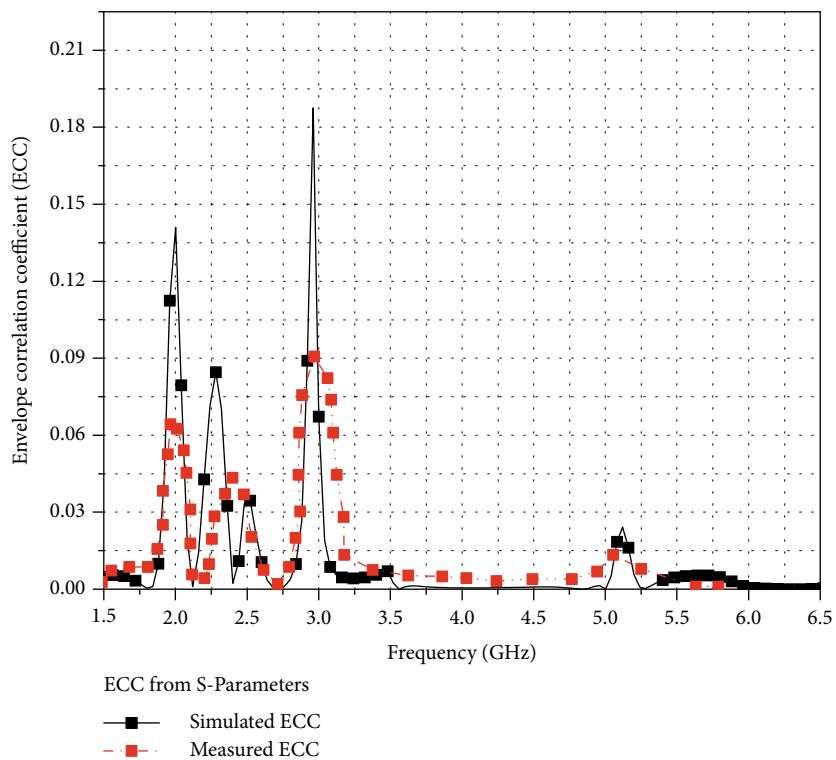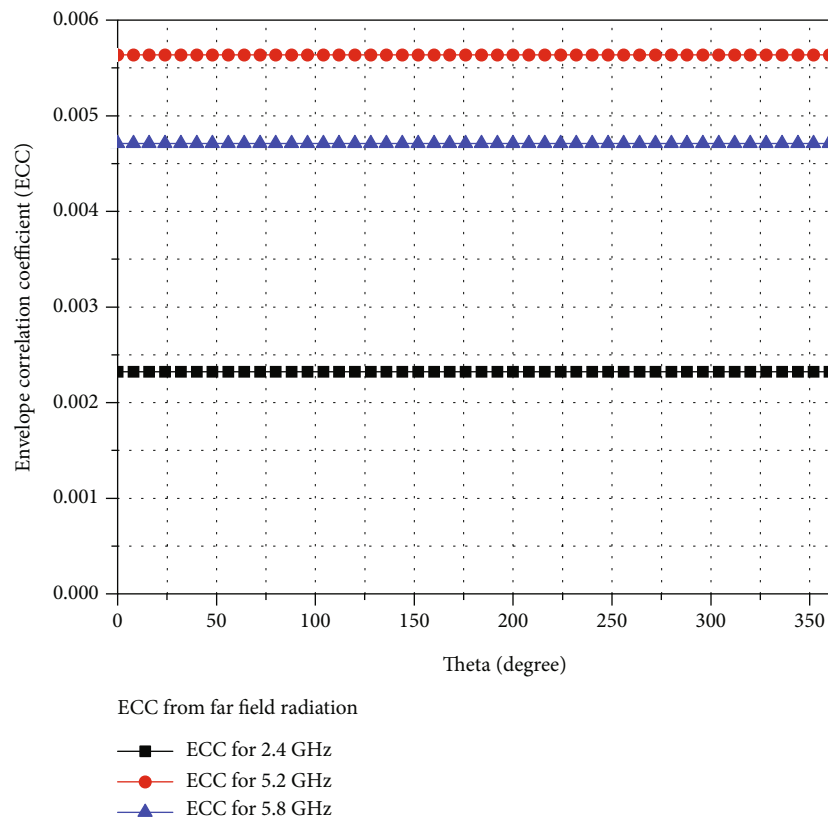
(b)

Figure 19: Continued.
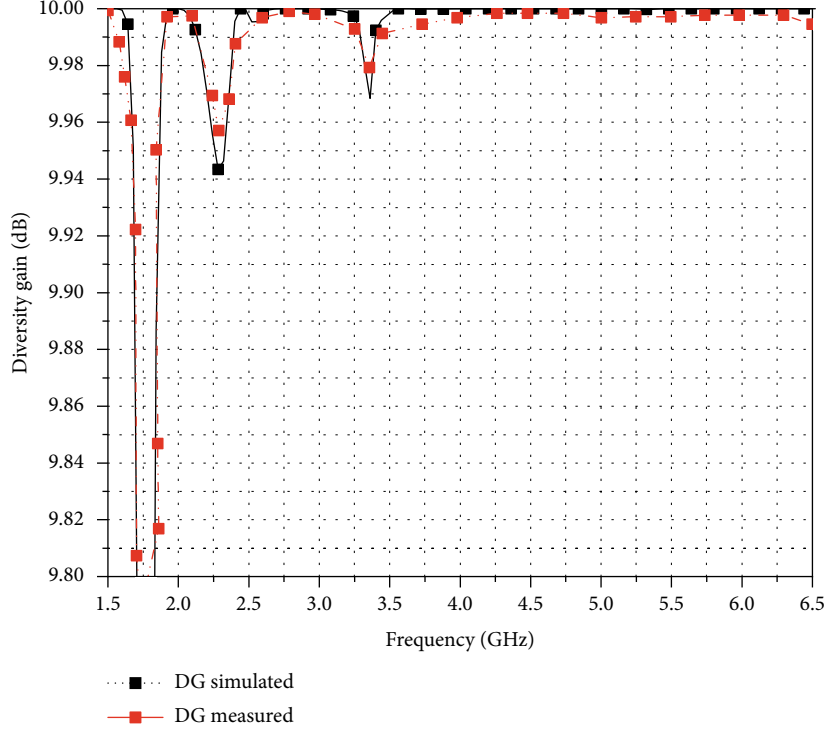
(c)

Figure 19: (a) Simulated and measured ECC from S parameter. (b) ECC for 2.4 GHz, 5.2 GHz, and 5.8 GHz from far field radiation. (c) Simulated and measured DG.

Table 2: Summarized ECC and DG parameters.

	Band 1	Band 2	Band 3
Frequency of operation	2.39 GHz	5.23 GHz	5.84 GHz
ECC (from S parameters)	0.002	0.005	0.004
ECC (from far field radiation)	0.0023	0.0056	0.0047
DG	9.99	10	10

3.2.2. Gain, Efficiency, and Radiation Pattern.

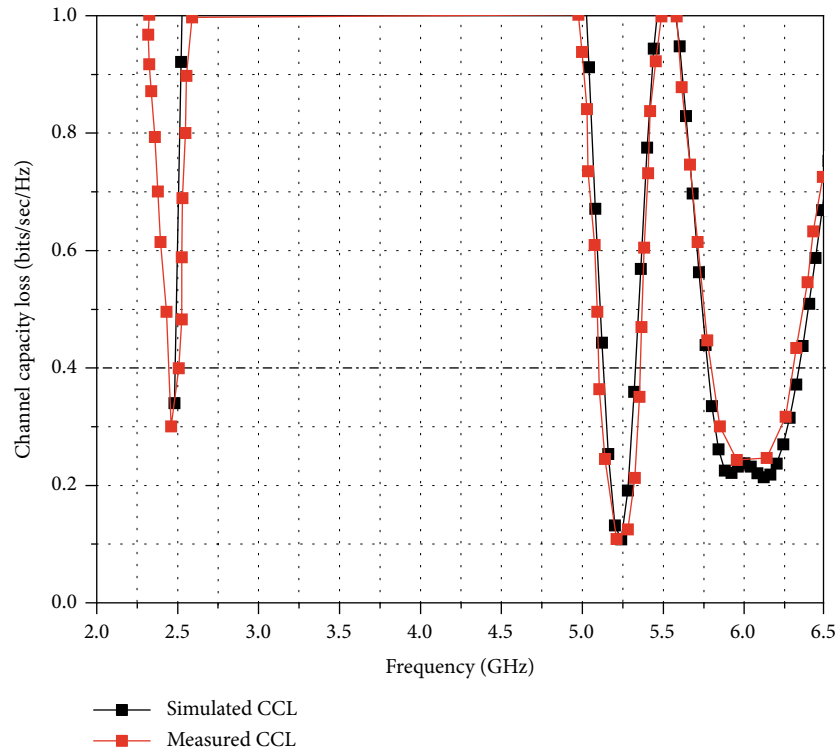The gain and radiation pattern of the proposed MIMO antenna is measured in an anechoic chamber with the help of a particular antenna measurement setup. Figure 17(b) shows the plot of simulated and measured gain and radiation efficiency. Both these parameters explain how well the designed antenna performs. The maximum gain attained by the antenna is 7.17 dBi at 5.28 GHz. It is observed that the gain is lower at lower frequencies. This is because the antenna becomes smaller with respect to the wavelength at lower frequencies. Gain at 2.4 GHz is 1.893 dBi and at 5.84 GHz, gain attained is 6.71 dBi. The radiation efficiencies are 65.74% (2.4 GHz), 84.75% at 5.28 GHz, and 92.3% at 5.84 GHz.

The radiation pattern for the E-plane and H-plane at all the three resonant frequencies are as shown in Figure 18. Figure 18(a) is the radiation pattern at 2.4 GHz, Figure 18(b) is the pattern for 5.2 GHz, and Figure 18(c) is the radiation pattern at 5.8 GHz.

3.3. MIMO Diversity Parameters.

MIMO antennas are analyzed with a set of diversity parameters as the envelope correlation coefficient (ECC), the diversity gain (DG), total active reflection coefficient (TARC), and channel capacity loss (CCL). Each of these has be evaluated below for the proposed dual-element, triband MIMO antenna.

3.3.1. Envelope Correlation Coefficient.

When multiple antennas are used simultaneously, the correlation between the received signals helps in analyzing the performance of the system. The far field radiation characteristics helps in evaluating ECC by

$$\text{ECC} = \frac{\left| \int\int_{4\pi} \vec{F}_1((\theta, \varnothing)) \times \vec{F}_2((\theta, \varnothing)) d\Omega \right|^2}{\left| \int\int_{4\pi} \left| \vec{F}_1((\theta, \varnothing)) \right|^2 d\Omega \times \int\int_{4\pi} \left| \vec{F}_2((\theta, \varnothing)) \right|^2 d\Omega \right|^2}.$$

(7)

(a)
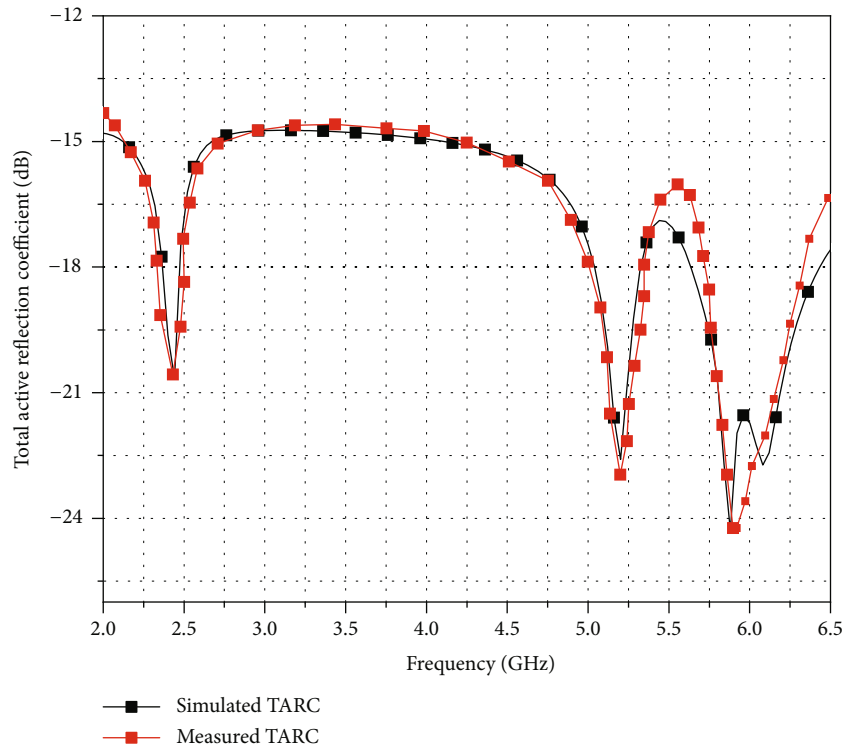
(b)

FIGURE 20: Diversity parameters of proposed MIMO. (a) Simulated and measured CCL. (b) Simulated and measured TARC.

The far field radiation characteristics of port 1 and port 2 are represented as F_1 and F_2. Ideally, the preferred value of ECC is 0, but for practical MIMO antenna systems, ECC less than 0.5 is accepted as acceptable performance.

3.3.2. Diversity Gain. The diversity gain is another parameter of interest in MIMO systems. DG is easily calculated from ECC using Equation (8). The value of DG needs to be very close to 10 dB for the operating bands in a well

TABLE 3: Multiband MIMO current state of arts.

Ref. no	No. of ports	Bandwidth/resonant frequency	Isolation	Technique used (multibanding and isolation)	ECC	Size
[29]	4	(3.72-3.82) GHz (4.65-4.76) GHz (6.16-6.46) GHz	>16 dB	Slots cut in the square shaped patch	<0.1	32 mm × 32 mm
[18]	4	(2.29-2.49) GHz (2.85-3.04) GHz (5.61-5.80) GHz	>18 dB	Square-shaped CSRR in DGS and use of metamaterial	<0.01	106.6 mm × 106.6 mm
[19]	2	2.9 GHz 4.3 GHz 7.7 GHz	>26.55 dB	DGS and Vias	<0.0001	64 mm × 30 mm
[23]	4	2.4 GHz 3.66 GHz 5.5 GHz	>14 dB	Slots in the DGS and SRR as parasitic element.	—	40 mm × 40 mm
[20]	4	(2.25-2.41) GHz (3.36-3.65) GHz (4.7-6.25) GHz	>18 dB	Antenna element geometry	<0.001	48 mm × 48 mm
[21]	2	(2.25-3.15) GHz (4.89-5.95) GHz	>15 dB	Slits in the patch, rectangular stub, and DGS	<0.01	50 mm × 50 mm
[30]	4	(3.3-3.84) GHz (4.61-5.91) GHz	>15 dB	Antenna geometry	<0.02	14.9 mm × 7 mm (single element)
[31]	8	(3.3-4.2) GHz (4.8-5) GHz	>10 dB	T-shaped decoupling stubs	<0.12	18.6 mm × 7 mm
[32]	4	(3.4-3.6) GHz (4.8-5) GHz	>16.5 dB	Slits and parasitic patch	<0.01	150 mm × 75 mm
[33]	4	(2-3) GHz (3.4-3.9) GHz (4.4-5.2) GHz	>20 dB	Sierpinski triangle fractal array	<0.01	30 × 40 mm
[34]	10	(3.3-4.2) GHz (4.8-5.0) GHz	>10 dB	Double T-shaped antenna	<0.12	150 mm × 80 mm
[35]	18	(3.4-3.6) GHz	>20 dB	Open-ended slots in the ground plane	<0.32	150 mm × 80 mm
[36]	1	(2.1-3.3) GHz (3.6-5) GHz (6-10.6) GHz	NA	Defected ground compact electromagnetic band gap	NA	42 mm × 50 mm
[37]	2	(2.6-3.3) GHz (3.6-4.7) GHz (6-10.6) GHz	>15 dB	Mushroom electromagnetic band gap arrangements	<0.02	58 mm × 45 mm
Proposed system	2	2.4 GHz 5.2GHz 5.8GHz	>18 dB	CSRR in the DGS	<0.02	40 mm × 40 mm

performing MIMO.

$$DG = 10\sqrt{1 - (ECC)^2}. \tag{8}$$

The ECC and DG plot for the proposed MIMO is shown in Figure 19. Both the measured and simulated ECC are well below 0.5 for this MIMO antenna, and the DG for the operating bands are close to 10. ECC has also been calculated from far field radiation pattern as shown in Figure 19(b). Table 2 summarizes the ECC and DG values for all the three operational bands.

3.3.3. Channel Capacity Loss. CCL is the parameter used to measure the information transmission rate of the wireless channel and CCL should be less than 0.5 bits/sec/Hz for a good communication system. The channel capacity loss for a system is calculated from

$$CCL = -\log_2 \det(\varphi^R), \tag{9}$$

where φ^R is the performance of the MIMO antenna and is given as in

$$\varphi^R = \begin{bmatrix} \rho_{ii} & \rho_{ij} \\ \rho_{ji} & \rho_{jj} \end{bmatrix}. \tag{10}$$

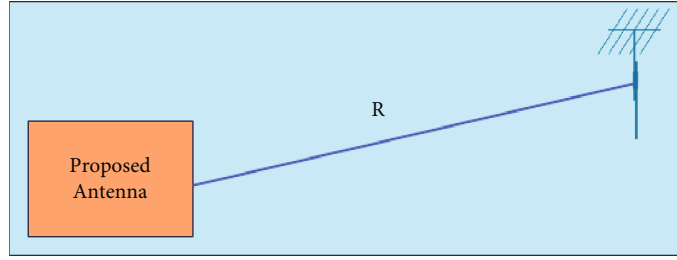The CCL values are 0.34 bits/sec/Hz for 2.39 GHz, 0.108 bits/sec/Hz for 5.23 GHz, and 0.261 bits/sec/Hz for

FIGURE 21: Block diagram for experimental setup for measurement of antenna range.
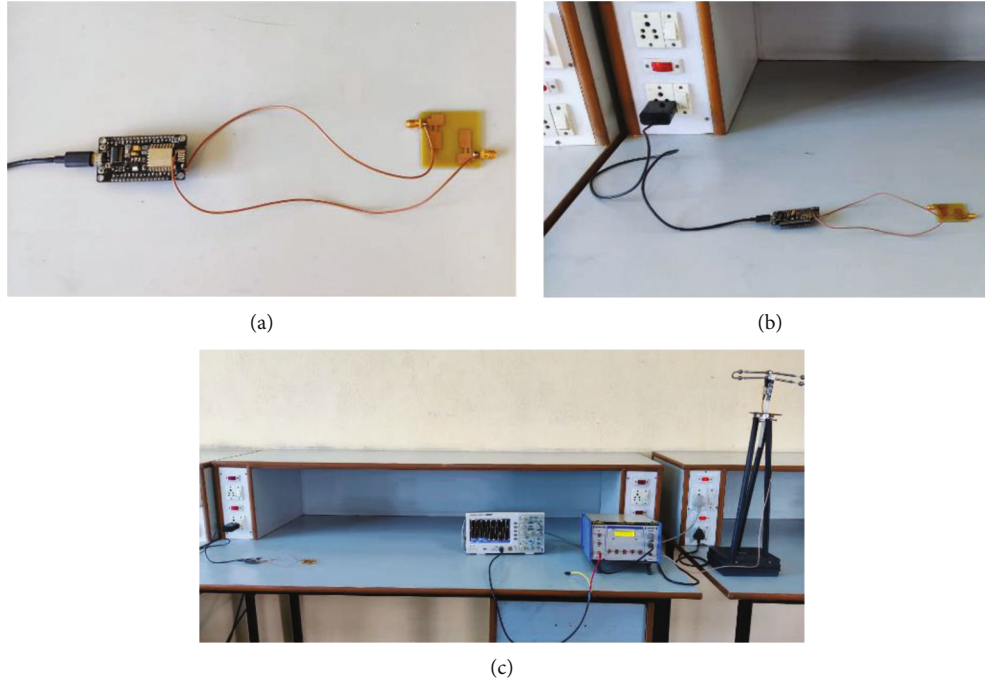

(a)

(b)

(c)

FIGURE 22: Experimental setup for measurement of antenna range. (a) Designed antenna connected to ESP8266 module. (b) Designed antenna excited. (c) The performance of designed antenna analyzed with reference to Yagi-Uda antenna.

5.84 GHz. The plot of simulated and measured CCL is shown in Figure 20(a).

3.3.4. Total Active Reflection Coefficient. TARC is another major parameter to study the performance of a MIMO antenna system. TARC studies the diversity performance while multiple antennas are working simultaneously. TARC, in other words, can be considered the return loss of a MIMO antenna system. TARC can be calculated from the formulation given as

$$\text{TARC} = \sqrt{\frac{\left|S_{11} + S_{12}\,e^{j\theta}\right|^2 + \left|S_{21} + S_{22}\,e^{j\theta}\right|^2}{2}}, \quad (11)$$

where θ is the difference in phase between the excitation signals.

For a well performing MIMO antenna, TARC is expected to be less than 0 dB. In this proposed antenna, TRAC is less than -18 dB for all the operational bandwidth which concludes that the proposed MIMO has good diver-

sity performance. The simulated and measured TARC is shown in Figure 20(b).

Table 3 summarizes the current state of arts of similar multiband MIMO antennas.

3.4. Radiation Pattern Analysis. The Friis transmission equation relates the power received to the power transmitted between a transmitting and receiving antennas separated by a distance $R > 2d^2/\lambda$ where d is the largest dimension of either antenna. The Friis transmission formula is given as follows:

$$\frac{P_r}{P_t} = \left(\frac{\lambda}{4\pi R}\right)^2 G_r G_t, \quad (12)$$

where λ is the wavelength of free space in meter, P_r is the receiving antenna power in dBm, P_t is the transmitting antenna power in dBm, and G_t and G_r is the gain of the transmitting antenna and receiving antenna.

The representation of the set up to evaluate the performance of the antenna is shown in Figure 21. The experimental setup consists of the proposed transmitting microstrip

antenna and a standard Yagi-Uda antenna as shown in Figure 22.

The above Friis equation can be represented as

$$R^2 = \left[\left(\frac{\lambda}{4\pi} \right)^2 G_r G_t \right] \frac{P_t}{P_r}. \tag{13}$$

For a given transmitted power (P_t) radiated by proposed antenna, the received power (P_r) is being measured and the plot of R^2 verses P_t/P_r gives a straight line with slope equal to $\left[(\lambda/4\pi)^2 G_r G_t \right]$ as per Equation (12). As the receiving antenna is standard Yagi-Uda antenna so its gain (G_r) is known whereas the gain of transmitting antenna is easily obtained from the gain plot of the proposed antenna.

The range can be obtained as per Equation (13) and confirms a wider coverage area as indicated by the radiation efficiency.

4. Conclusion

IoT technology has evaded almost every field in the present day, and wireless communication technologies plays a vital role in the effective implementation of IoT systems. Modules like ESP8266 are widely used for various IoT applications. Multifrequency operational antennas with enhanced performance and reduced size are desired for many IoT and modern wireless applications. The paper suggests a dual-element, triband MIMO antenna with a microstrip line feed. The antenna is low profile and compact and built of FR4 substrate of size 40 mm × 40 mm. The simple and identical radiating patches with the CSRR embedded in the DGS provides three versatile operating frequencies of 2.4 GHz, 5.2 GHz, and 5.8 GHz. The antenna exhibits good isolation and stable gain and radiation characteristics and can be used for IEEE 802.11 a/b/g applications and other IoT systems connected to the above frequencies of operation. A peak gain of 3.56 dBi is attained for the proposed MIMO system. The MIMO diversity parameter requirements including DG > 9.8, ECC < 0.2, TARC < −10 dB, and CCL < 0.5 bits/s/Hz. This makes the proposed antenna a good candidate for IoT applications employing WLAN frequencies. The antenna has also been tested with standard Yadi-Uda antenna to analyze its performance when connected to ESP8266 module.

Data Availability

The data will be available upon request.

Conflicts of Interest

The authors declare that they have no known competing financial interest or personal relationships that could have appeared to influence the work reported in this paper.

References

[1] P. K. Malik, R. Singh, A. Gehlot, S. V. Akram, and P. K. Das, "Village 4.0: digitalization of village with smart internet of things technologies," *Computers & Industrial Engineering*, vol. 165, article 107938, 2022.

[2] A. Rahim and P. K. Malik, "Analysis and design of fractal antenna for efficient communication network in vehicular model," *Sustainable Computing: Informatics and Systems*, vol. 31, article 100586, 2021.

[3] A. Rahim, P. K. Malik, and V. A. Sankar Ponnapalli, "State of the art: a review on vehicular communications, impact of 5G, fractal antennas for future communication," in *Proceedings of First International Conference on Computing, Communications, and Cyber-Security (IC4S 2019)*, pp. 3–15, Singapore, 2020.

[4] P. K. Malik, R. Sharma, R. Singh et al., "Industrial internet of things and its applications in industry 4.0: state of the art," *Computer Communications*, vol. 166, pp. 125–139, 2021.

[5] A. S. Duggal, P. K. Malik, A. Gehlot et al., "A sequential roadmap to industry 6.0: exploring future manufacturing trends," *IET Communications*, vol. 16, no. 5, pp. 521–531, 2022.

[6] P. Varga, J. Peto, A. Franko et al., "5G support for industrial IoT applications—challenges, solutions, and research gaps," *Sensors*, vol. 20, no. 3, p. 828, 2020.

[7] A. Sabban, "Small new wearable antennas for IOT, medical and 5G applications," in *2020 14th European Conference on Antennas and Propagation (EuCAP)*, pp. 1–5, Copenhagen, Denmark, 2019.

[8] T. Rashid, M. N. Hasan, and P. S. Mazumdar, "An L-slot compact antenna for medical, wearable device and IoT applications," in *2021 International Conference on Information and Communication Technology for Sustainable Development (ICICT4SD)*, pp. 100–104, Dhaka, Bangladesh, 2021.

[9] C. C. Wan and S. W. Su, "Dual-feed, dipole antenna system for 2.4/5.2/5.8-GHz, tri-band WLAN laptop applications," *Progress in Electromagnetics Research C*, vol. 102, pp. 175–185, 2020.

[10] P. B. Nayak, R. Endluri, S. Verma, and P. Kumar, "A novel compact dual-band antenna design for WLAN applications," 2021, https://arxiv.org/abs/2106.13232.

[11] X. L. Sun, L. Liu, S. W. Cheung, and T. I. Yuk, "Dual-band antenna with compact radiator for 2.4/5.2/5.8 GHz WLAN applications," *IEEE Transactions on Antennas and Propagation*, vol. 60, no. 12, pp. 5924–5931, 2012.

[12] R. Roges and P. K. Malik, "Planar and printed antennas for Internet of Things-enabled environment: opportunities and challenges," *International Journal of Communication Systems*, vol. 34, no. 15, article e4940, 2021.

[13] A. Kaur and P. K. Malik, "Multiband elliptical patch fractal and defected ground structures microstrip patch antenna for wireless applications," *Progress In Electromagnetics Research B*, vol. 91, pp. 157–173, 2021.

[14] M. Li, B. G. Zhong, and S. W. Cheung, "Isolation enhancement for MIMO patch antennas using near-field resonators as coupling-mode transducers," *IEEE Transactions on Antennas and Propagation*, vol. 67, no. 2, pp. 755–764, 2019.

[15] M. Li, L. Jiang, and K. L. Yeung, "A general and systematic method to design neutralization lines for isolation enhancement in MIMO antenna arrays," *IEEE Transactions on Vehicular Technology*, vol. 69, no. 6, pp. 6242–6253, 2020.

[16] N. Agrawal and M. Gupta, "Isolation enhancement techniques for UWB-MIMO system: a review," in *2020 International Conference on Power Electronics & IoT Applications in Renewable Energy and its Control (PARC)*, pp. 113–117, Mathura, India, 2020.

[17] S. Chouhan, D. K. Panda, M. Gupta, and S. Singhal, "Multiport MIMO antennas with mutual coupling reduction techniques for modern wireless transreceive operations: a review," *International Journal of RF and Microwave Computer-Aided Engineering*, vol. 28, no. 2, article e21189, 2018.

[18] M. Aminu-Baba, M. K. A. Rahim, F. Zubir et al., "A compact triband miniaturized MIMO antenna for WLAN applications," *AEU-International Journal of Electronics and Communications*, vol. 136, article 153767, 2021.

[19] S. R. Pasumarthi, J. B. Kamili, and M. P. Avala, "Design of triband MIMO antenna with improved isolation using DGS and Vias," *Wireless Personal Communications*, vol. 110, no. 3, pp. 1523–1532, 2020.

[20] P. V. Naidu, M. B. Dhanekula, K. M. Almustafa, A. Kumar, K. A. Meerja, and S. H. Akkapanthula, "Design and performance analysis of MAZE shaped quad port ACS fed tri band MIMO antenna for V2V and multi band applications," *AEU-International Journal of Electronics and Communications*, vol. 134, article 153676, 2021.

[21] Y. Dou, Z. Chen, J. Bai, Q. Cai, and G. Liu, "Two-port CPW-fed dual-band MIMO antenna for IEEE 802.11 a/b/g applications," *International Journal of Antennas and Propagation*, vol. 2021, Article ID 5572887, 8 pages, 2021.

[22] S. Mohker, A. Naik, A. Parmar, and L. Malviya, "Design of bandstop filter using double dumbbell shaped CSRR in ground," in *2022 IEEE 11th International Conference on Communication Systems and Network Technologies (CSNT)*, pp. 54–59, Indore, India, 2022.

[23] V. Rajeshkumar and R. Rajkumar, "SRR loaded compact tri-band MIMO antenna for WLAN/WiMAX applications," *Progress In Electromagnetics Research Letters*, vol. 95, pp. 43–53, 2021.

[24] I. Elfergani, J. Rodriguez, A. Iqbal, M. Sajedin, C. Zebiri, and R. A. AbdAlhameed, "Compact millimeter-wave MIMO antenna for 5G applications," in *2020 14th European Conference on Antennas and Propagation (EuCAP)*, pp. 1–5, Copenhagen, Denmark, 2020.

[25] A. Iqbal, A. Altaf, M. Abdullah, M. Alibakhshikenari, E. Limiti, and S. Kim, "Modified U-shaped resonator as decoupling structure in MIMO antenna," *Electronics*, vol. 9, no. 8, p. 1321, 2020.

[26] N. Muchhal, M. Elkhouly, R. Z. Vintimilla, A. Chakraborty, and S. Srivastava, "Design of hybrid fractal integrated half mode SIW band pass filter with CSRR and Minkowski defected ground structure for sub-6 GHz 5G applications," *Photonics*, vol. 9, no. 12, p. 898, 2022.

[27] G. Soundarya and N. Gunavathi, "Compact dual-band SIW bandpass filter using CSRR and DGS structure resonators," *Progress In Electromagnetics Research Letters*, vol. 101, pp. 79–87, 2021.

[28] P. K. Keshri, S. K. Sahu, and R. Chandel, "CSRR-loaded compact quad port MIMO diversity antenna for UWB applications," *IETE Journal of Research*, pp. 1–11, 2021.

[29] R. Krishnamoorthy, A. Desai, R. Patel, and A. Grover, "4 element compact triple band MIMO antenna for sub-6 GHz 5G wireless applications," *Wireless Networks*, vol. 27, no. 6, pp. 3747–3759, 2021.

[30] J. Huang, G. Dong, Q. Cai, Z. Chen, L. Li, and G. Liu, "Dual-band MIMO antenna for 5G/WLAN mobile terminals," *Micromachines*, vol. 12, no. 5, p. 489, 2021.

[31] L. Cui, J. Guo, Y. Liu, and C. Y. D. Sim, "An 8-element dual-band MIMO antenna with decoupling stub for 5G smartphone applications," *IEEE Antennas and Wireless Propagation Letters*, vol. 18, no. 10, pp. 2095–2099, 2019.

[32] J. Huang, G. Dong, J. Cai, H. Li, and G. Liu, "A quad-port dual-band MIMO antenna array for 5G smartphone applications," *Electronics*, vol. 10, no. 5, p. 542, 2021.

[33] S. H. Ghadeer, S. K. A. Rahim, M. Alibakhshikenari et al., "An innovative fractal monopole MIMO antenna for modern 5G applications," *AEU-International Journal of Electronics and Communications*, vol. 159, article 154480, 2023.

[34] N. Jaglan, S. D. Gupta, B. K. Kanaujia, and M. S. Sharawi, "10 element sub-6-GHz multi-band double-T based MIMO antenna system for 5G smartphones," *IEEE Access*, vol. 9, pp. 118662–118672, 2021.

[35] N. Jaglan, S. D. Gupta, and M. S. Sharawi, "18 element massive MIMO/diversity 5G smartphones antenna design for sub-6 GHz LTE bands 42/43 applications," *IEEE Open Journal of Antennas and Propagation*, vol. 2, pp. 533–545, 2021.

[36] N. Jaglan, B. K. Kanaujia, S. D. Gupta, and S. Srivastava, "Design of band-notched antenna with DG-CEBG," *International Journal of Electronics*, vol. 105, no. 1, pp. 58–72, 2018.

[37] N. Jaglan, B. K. Kanaujia, S. D. Gupta, and S. Srivastava, "Dual band notched EBG structure based UWB MIMO/diversity antenna with reduced wide band electromagnetic coupling," *Frequenz*, vol. 71, no. 11-12, pp. 555–565, 2017.